Topology Optimization of Electromagnetic Devices Using Digital Annealer

Akito Maruo[1,2], Takeshi Soeda[1], and Hajime Igarashi[2], *IEEE Member*

[1] FUJITSU LTD., Atsugi 243-0197, Japan, maruo.akito@fujitsu.com
[2] Graduate School of Information Science and Technology, Hokkaido University, Sapporo 060-0814, Japan

Topology optimization has been formulated as a quadratic unconstrained binary optimization (QUBO) problem that can be solved by Digital Annealer (DA) and quantum computers, which can realize massive parallelization. It is shown that the 3D topology optimization (TO) of a permanent magnet, with 600 unknowns, is successfully performed by the DA with the aid of the finite element method for field computations. Moreover, it is shown to perform TO of a magnetic core, with 758 unknowns, in such a way that the QUBO and field problems are iteratively solved to determine the optimal solution wherein the magnetic field and optimal core structure are self-consistent.

***Index Terms*— Design optimization, Digital Annealer, Magnetic shield, Quadratic unconstrained binary optimization, Topology optimization.**

I. Introduction

TOPOLOGY optimization (TO) has attracted significant attention in recent years because it can provide novel machine structures with outstanding performance. TO does not require the setting of shape parameters in contrast to the conventional parameter optimization. TO can be classified into two types of methods: (i) approaches, such as the density method and level set method, based on sensitivity computation, and (ii) the on-off method, which determines the binary states of small cells using stochastic optimization algorithms. In this study, we employ the latter method because it can perform a global search without performing sensitivity computations. However, the on-off method requires a heavier computational burden than (i). This drawback can be alleviated by using parallel computations.

In this study, we show that TO can be formulated as a quadratic unconstrained binary optimization (QUBO) problem, which can be solved by Fujitsu Quantum-inspired Computing Digital Annealer™ (DA) [1-5] and quantum computers, whose performance is expected to rapidly increase. It is expected that the proposed method can solve a large-scale TO problems which cannot be solved effectively by the conventional methods. Using DA, we can solve fully connected QUBO problems using an algorithm based on simulated annealing (SA) with massive parallel computations. The authors have shown that DA successfully optimizes the two-dimensional structure of a Halbach magnet array [4]. In this study, we extend this method to solve TO for a permanent magnet (PM) with assumed magnetization. Moreover, we extend the method to apply TO to the design of magnetic cores, whose magnetization is determined by field computations.

It is necessary to formulate the problems in QUBO forms for ease of use in DA as well as quantum computing, whose performance is expected to surpass that of Neumann-type computers. The scientific novelty of this study is that TO is initially formulated as a QUBO problem for DA and quantum computing.

Manuscript received April 1, 2015; revised May 15, 2015 and June 1, 2015; accepted July 1, 2015. Date of publication July 10, 2015; date of current version July 31, 2015. (Dates will be inserted by IEEE; "published" is the date the accepted preprint is posted on IEEE Xplore®; "current version" is the date the typeset version is posted on Xplore®). Corresponding author: A. Maruo (e-mail: maruo.akito@fujitsu.com).

Digital Object Identifier (inserted by IEEE).

II. Topology Optimization Of Permanent Magnet

A. Optimization Problem

We consider the TO of the two-dimensional PM shown in Fig. 1. The purpose of this problem is to determine the PM structure such that the magnetic flux density $B_y^{(j)}$ at points P_j, $j = 1,2,\dots,N_p$, on the observation line matches the predetermined value. The PM region is divided into small PMs for the on-off method. The binary variable $s_i \in \{0,1\}$ denotes the material attribute of the i-th element in the PM region; the magnet and air correspond to states $s_i = 1, 0$, respectively. We determine the PM state vector $\boldsymbol{s}$ such that B_y along the observation line becomes sinusoidal. The small PMs are assumed as magnetized parallel to the y-axis, as shown in Fig. 1. We minimize the squared error between $B_y^{(j)}$ generated by the PMs and value $B_0^{(j)}$ defined by

$$F = \sum_{j=1}^{N_p} \left(B_y^{(j)} - B_0^{(j)} \right)^2 = \sum_{j=1}^{N_p} \left(\sum_{i=1}^{N_m} B_y^{(i,j)} s_i - B_0^{(j)} \right)^2 \qquad (1)$$

where N_m and $B_y^{(i,j)}$ denote the number of small PMs and magnetic flux density in y-direction generated by the i-th magnet at P_j, respectively. The coefficients $B_y^{(i,j)}$ are computed using Biot–Savart's law [4] and given to DA. Given that $B_y^{(i,j)}$ are the linear functions of s_j, (1) can be represented by a QUBO problem, which is solved by DA to determine s_j. Furthermore, the optimal PM shape is expected to be symmetric because we assume a sinusoidal magnetic field distribution in this problem. Hence, variables s_i of QUBO are assumed to exhibit a

symmetric distribution along the x-axis.

The on-off method can lead to checkerboard-like shapes that cannot be manufactured [6]. Therefore, we introduce a regularization term for Equation (1). Specifically, we impose the linkage constraints used in the game of Reversi. The concatenation constraints for vertical, horizontal, and diagonals (\) and (/) are as follows:

$$
\begin{aligned}
C_w &= \sum_{j=1}^{N_y}\sum_{i=2}^{N_x-1}\left(s_{(i+j\times N_x)-1}-s_{(i+j\times N_x)}\right)\\
&\quad\times\left(s_{(i+j\times N_x)+1}-s_{(i+j\times N_x)}\right)\\
C_h &= \sum_{j=2}^{N_y-1}\sum_{i=1}^{N_x}\left(s_{(i+j\times N_x)-N_x}-s_{(i+j\times N_x)}\right)\\
&\quad\times\left(s_{(i+j\times N_x)+N_x}-s_{(i+j\times N_x)}\right)\\
C_b &= \sum_{j=2}^{N_y-1}\sum_{i=2}^{N_x-1}\left(s_{(i+j\times N_x)-N_x-1}-s_{(i+j\times N_x)}\right)\\
&\quad\times\left(s_{(i+j\times N_x)+N_x+1}-s_{(i+j\times N_x)}\right)\\
C_s &= \sum_{j=2}^{N_y-1}\sum_{i=2}^{N_x-1}\left(s_{(i+j\times N_x)-N_x+1}-s_{(i+j\times N_x)}\right)\\
&\quad\times\left(s_{(i+j\times N_x)+N_x-1}-s_{(i+j\times N_x)}\right)
\end{aligned}
\tag{2}
$$

where N_x and N_y denote the numbers of small PMs in the x- and y-*axes*, respectively. The aforementioned constraint terms, which are positive unless the constraint is satisfied and zero if it is satisfied, are added to (1).

$$
F' = F + \alpha_w C_w + \alpha_h C_h + \alpha_b C_b + \alpha_s C_s \rightarrow \min. \tag{3}
$$

where, $\alpha_w, \alpha_h, \alpha_b, \alpha_s$ denote the weight coefficients.

Next, we consider the TO of a three-dimensional PM where the two-dimensional structure is extruded along the z-axis. Furthermore, symmetry is considered in the z-axis direction as shown in Fig. 2. We consider a PM consisting of four layers, where the uppermost and lower-most layers and the middle two layers have the same structures. Given that the magnetic field varies along the z-axis, the observation lines L_i are placed at the center of each layer. The magnet shape is optimized such that the total error along the observation lines is minimized.

B. Optimization Results

TO is applied to the two-dimensional PM as shown in Fig.1. We solve TO problem (3) using DA, where N_x, N_y, and N_p are set to 40, 20, and 21, respectively. The PM is subdivided into small square PMs with a side length of 10 mm, and the distance between the magnet region and observation line is set to 10 mm. Fig. 3 shows the optimization results. As shown in Fig. 3 (b), the desired magnetic flux density is generated by the optimized PM. The maximum error is $\Delta B_y = 3.24$ mT. The optimized shape has a fan-shaped spread toward the observation line. Moreover, it has a smooth boundary owing to concatenation constraints.

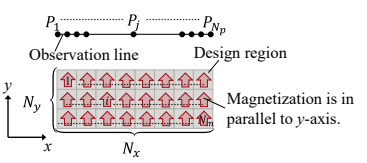

Fig. 1. Analysis object.

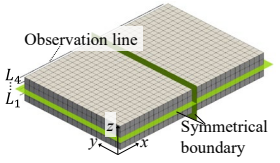

Fig. 2. 3D analysis model.

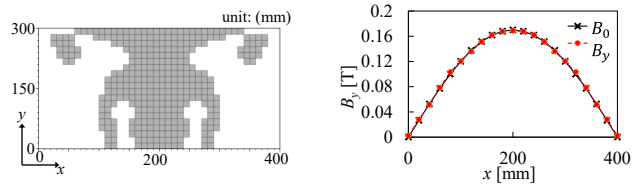

(a) (b)

Fig. 3. 2-D Optimization results (40 × 20 × 1 model). (a) Shape. (b) Magnitude of the magnetic flux density along the observation line.

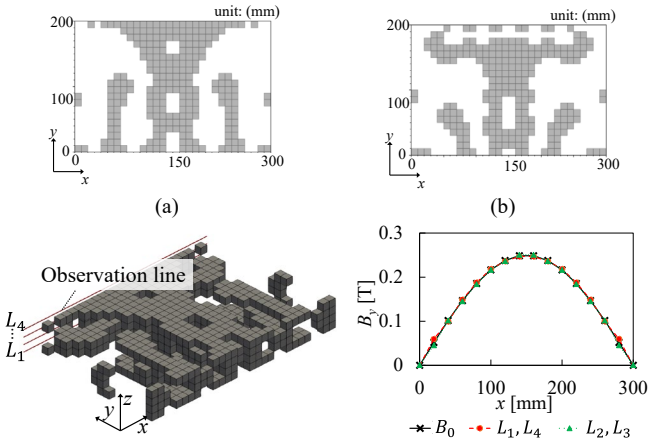

(a) (b) (c) (d)

Fig. 4. 3-D Optimization results (30×20×4 model). (a) Layer 1, Layer 4. (b) Layer 2, Layer 3. (c) Overall view. (d) Magnitude of the magnetic flux density along the observation line.

TO is then applied to the three-dimensional PM shown in Fig.2. We solve (3) using DA, where N_x, N_y, and N_z are set as 30, 20, and 4, respectively. We have 600 unknowns in total. We place 16 sampling points along one observation line such that the total number of sampling points N_p is 64. Fig. 4 shows the optimization results. The upper and lower most layers have a fan-shaped structure similar to that of the two-dimensional PM. The middle layers have small island PMs that contribute to the uniformity of B_y in the z-axis direction. The resulting magnetic flux density is in good agreement with the predetermined flux density. The maximum error is $\Delta B_y = 7.92$ mT.

III. Topology Optimization Of Magnetic Core

The method described in Section II is extended to perform the TO of a magnetic core. We use the finite element method (FEM) for magnetostatic field computation, where the cells in the design region correspond to the finite elements. The material attribute of the cell is identified as a magnetic core (air) if $s_i = 1$ (0). The difference between the problems for the PM and magnetic core is that the magnetization $\boldsymbol{M}_j, j = 1,2,\ldots$ in the cells must be determined in the latter. In the first stage, assuming that $s_i = 1$ in all the cells in the design region, we compute the magnetic flux density distribution using the FEM.

Next, $\boldsymbol{M}_j$ in the design region is obtained from the resultant magnetic flux density distribution. We then compute the magnetic flux density generated by $\boldsymbol{M}_j$ using Biot–Savart's law. Given that DA can only deal with QUBO forms, we convert the topology optimization problem to QUBO. The binary variable s_i is determined by solving the QUBO using the DA. Furthermore, to suppress the complexity of the material distribution, the distribution is smoothed by a spatial filter, where the density is weighted with distance [7]. A flowchart of the proposed method is presented in Fig. 5.

Once $\boldsymbol{M}_j$ in the cells is assumed, s_j is determined using the DA to minimize the cost function. After determining s_j, we update the magnetization by performing FE computation of the magnetic field with a conventional computer. This process is repeated until convergence.

A. Optimization Problem

We consider the TO of a two-dimensional magnetic shielding system shown in Fig. 6, where the design region is divided into 758 elements. The aim of this problem is to obtain a magnetic shield configuration that minimizes the magnetic flux density in the target region with a minimal amount of magnetic material. Fig. 7 shows the BH curve of the magnetic material.

B. Determination of Magnetization

The magnetization vector $\boldsymbol{M}_j$ in the cell, where $s_j = 1$, is obtained from the magnetic flux density distribution, $\boldsymbol{B}_j$, computed from the FEM analysis as follows:

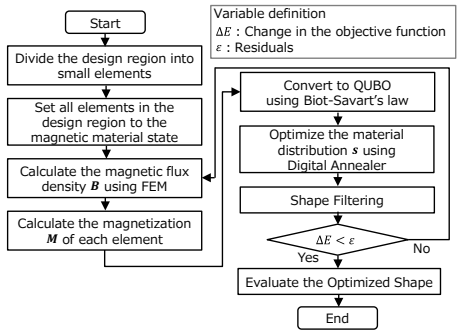

Fig. 5. Flowchart of the proposed method.

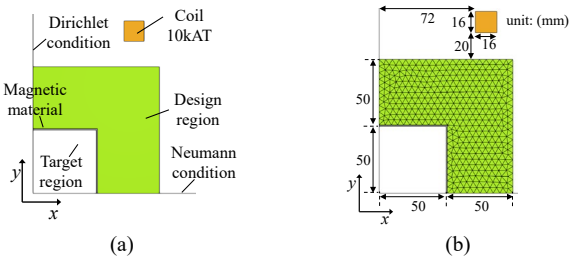

Fig. 6. Optimization model. (a) Whole. (b) Divided elements and size.

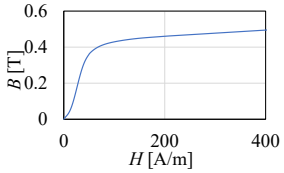

Fig. 7. BH curve of the magnetic material.

$$\boldsymbol{M}_j = \frac{\mu_r - 1}{\mu_0 \mu_r} \boldsymbol{B}_j \tag{4}$$

where μ_0 and μ_r denote the permeability of air and relative permeability of the magnetic core, respectively. In the optimization process, we assign $\boldsymbol{M}_j$ to all elements in the design region. If the element is air ($s_i = 0$), we assume the newest value for $\boldsymbol{M}_j$ computed in the previous steps.

C. QUBO Formulation

The magnetic flux density $\boldsymbol{B}_k$ of the k-th element in the target region is computed using Biot–Savart's law [8], where the field source is as follows:

$$\boldsymbol{B}_k = \frac{\mu_0}{2\pi} \sum_{i=1}^{N_D} s_i \left(2 \frac{\boldsymbol{M}_i \cdot \boldsymbol{R}_{i,k}}{\boldsymbol{R}_{i,k}^4} \boldsymbol{R}_{i,k} - \frac{\boldsymbol{M}_i}{\boldsymbol{R}_{i,k}^2} \right) \Delta S_i + \frac{\mu_0}{2\pi} \sum_{j=1}^{N_C} \frac{\boldsymbol{J}_j \times \boldsymbol{R}_{j,k}}{\boldsymbol{R}_{j,k}^2} \Delta S_j \tag{5}$$

where $\boldsymbol{R}$, $\boldsymbol{J}$, and ΔS denote the position vector, current density, and element area, respectively. Moreover, N_D and N_C denote the total number of elements in the design and coil regions, and i, j, k denote the indexes relevant to the elements in the design, coil, and target regions, respectively. The optimization problem of the magnetic shield can be expressed in the following QUBO form:

$$E = \frac{\alpha}{E_1} \sum_{k=1}^{N_T} (\boldsymbol{B}_k \Delta S_k)^2 + \frac{\beta}{E_2} \sum_{i=1}^{N_D} \Delta S_i s_i \rightarrow \min. \tag{6}$$

where E_1, E_2, and N_T denote the square of the magnetic flux density in the target region without shielding, area of the design region, and number of elements in the target region, respectively. Moreover, α and β denote weighting coefficients. The first and second terms in (6) denote the normalized magnitude of the magnetic flux density in the target region and total amount of magnetic shielding. When evaluating E in (6) using DA, the coefficients of s_i are computed before the optimization using a conventional computer and provided to the DA.

D. Optimization Results

By solving (6) using DA, we optimize the magnetic shield shape, where α and β are set to 0.95 and 0.05, respectively. Moreover, the filtering radius r_{min} was set to 7 [mm]. Fig. 8 shows the reference and optimization shape, where the area of the magnetic material is 1882 [mm^2] in both shapes. The optimal system has a small magnetic island near the coil, which acts as an outer shield. The width of the inner shield is thin near the symmetric axis and becomes thicker on the right side. This structure increases the magnetic resistance in the central region to guide the magnetic flux to the outer side with a lower magnetic resistance. Hence, the average magnetic flux density in the target region is reduced from 5.91×10^{-2} [mT] in (a) to

5.42×10^{-2}[mT] in (b) without an increase in the amount of magnetic material. Fig. 9 shows the change in the value of E during the optimization using DA by the iterative process in Fig. 5. It converges sufficiently after 19 iterations. Moreover, FE computations are required to evaluate the final shape. Hence, 20 FE computations are performed for this optimization.

We compare the performance of the proposed method with that of the on-off method based on a Gaussian network (NGnet). The latter has been shown to be effective in the topology optimization of electronic devices such as motors [9]. In this method, we employ a shape function $y(\boldsymbol{x}, \boldsymbol{w}) = \sum_{m=1}^{N_G} w_m \{G_m(\boldsymbol{x}) / \sum_{n=1}^{N_G} G_n(\boldsymbol{x})\}$ for determining the material distribution in the design region is set, where w_m, $\boldsymbol{x}$ and $G_m(x)$ denote the weighting coefficients, position vector and the Gaussian function, respectively. From the value of y, we determine the material distribution in the design region as follows: $s_i = 1$, if $y(x_i, w) \geq 0$, $s_i = 0$ otherwise. Using a conventional computer, we determined the unknown parameters $\boldsymbol{w}$ by solving the optimization problem defined by $F_1 = B_{T\_ave}(\boldsymbol{w}) \rightarrow \min., F_2 = S_{mag}(\boldsymbol{w}) \rightarrow \min.,$ using NSGA-II [10], where B_{T_ave} and S_{mag} denote the average magnetic flux density in the target region and area of the magnetic material, respectively. The numbers of generations and individuals are set to 100 and 120, respectively. The crossover rate of NSGA-II is set to 0.9. The optimization results are shown in Fig. 10, where 96 Gaussians are placed as shown in Fig. 11 (a). We can find in Fig. 10 that B_{T_ave} and S_{mag} are in a trade-off relationship. As shown in Fig. 10, the solution of the proposed method is located on the Pareto front obtained by the NGnet. Fig. 11 (b) shows the shape of the solution on the Pareto front in Fig. 10, where we observe features similar to those in Fig. 8. The NGnet method requires 12,000 FE computations, whereas the proposed method only needs 20 FE computations. Although the problem size that is manageable for DA and quantum computers is still significantly smaller than that for conventional computers, current intensive research in this field can lead to significant improvements. Hence, the proposed method can be effectively used to solve engineering problems in the aforementioned conditions.

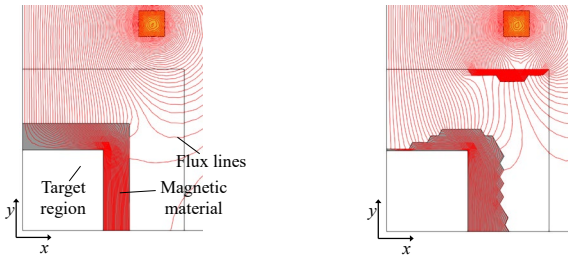

Fig. 8. Reference and Optimized shapes. (a) Reference. (b) Optimized.

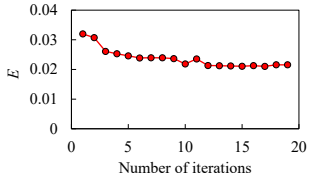

Fig. 9. Variation in E during optimization process.

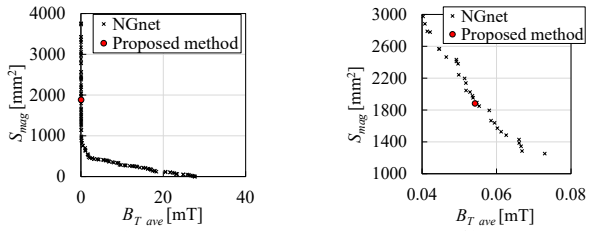

Fig. 10 . Optimization results. (a) Whole. (b) Part. $0.04 \leq B_{T_{ave}} \leq 0.08, 1000 \leq S_{mag} \leq 3000$.

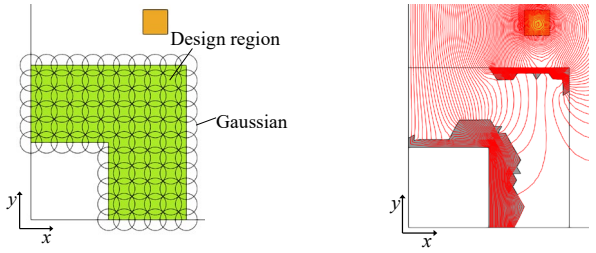

Fig. 11. Optimized result of on-off method based on NGnet. $B_{T\_ave} = 5.85 \times 10^{-2}$[mT] . $S_{mag} = 1881$[mm²]. (a) Contours of Gaussian functions. (b) Optimized shape and Flux lines.

IV. CONCLUSIONS

We proposed the QUBO formulation for the TO of PM and magnetic core for DA. Furthermore, the proposed formulation is valid for quantum computing [11]. The predetermined distribution of magnetic induction was successfully generated by the optimized PM. Moreover, the optimal magnetic shielding structure was obtained by the proposed method, where the magnetization and core topology were iteratively determined.

REFERENCES

[1] *Fujitsu Quantum-inspired Computing Digital Annealer*, Jan. 2022, [online] Available: https://www.fujitsu.com/global/services/business-services/digital-annealer/.

[2] A. Maliheh, *et al.*, "Physics-inspired optimization for quadratic unconstrained problems using a Digital Annealer," *Front. Phys.*, vol. 7, no. 48, 2019.

[3] S. Matsubara *et al.*, "Digital Annealer for High-Speed Solving of Combinatorial optimization Problems and Its Applications," *2020 25th Asia and S. Pac. Des. Autom. Conf. (ASP-DAC). ,* Beijing, China, 2020, pp. 667-672.

[4] A. Maruo *et al.*, "Optimization of planar magnet array using Digital Annealer," *IEEE Trans. Magn.*, vol. 56, no. 3, pp. 1-4, 2020.

[5] A. Maruo *et al.*, "Design optimization of coils and magnets in vibration energy harvester using Digital Annealer," *2020 19th Biennial Conf. on Electromagn. Field Comput. (CEFC)*, Pisa, Italy, 2020, pp. 1-4.

[6] O. Sigmund and J. Petersson, "Numerical instabilities in topology optimization: A survey on procedures dealing with checkerboards, mesh-dependencies and local minima," *Struct. Optim.*, vol. 16, no. 1, pp. 68-75, 1998.

[7] S. R. M. Almeida, *et al.*, "A simple and effective inverse projection scheme for void distribution control in topology optimization," *Struct. Multidisc Optim.*, vol. 39, no. 4, pp. 359–371, 2009.

[8] L. Urankar, "Vector potential and magnetic field of current-carrying finite arc segment in analytical form, Part III: Exact computation for rectangular cross section," *IEEE Trans. Magn.*, vol. 18, no. 6, pp. 1860-1867, 1982.

[9] T. Sato *et al.*, "Multimaterial topology optimization of electric machines based on normalized Gaussian network," *IEEE Trans. Magn.*, vol. 51, no. 3, pp. 1-4, Mar. 2015.

[10] K. Deb *et al.*, "A fast and elitist multiobjective genetic algorithm: NSGA-II" in *IEEE Trans. Evol. Comput.*, vol. 6, no. 2, pp. 182-197, 2002.

[11] L. Andrew, "Ising formulations of many NP problems," *Front. Phys.*, vol. 2, pp. 1-5, 2014.